Towards Alternative Approaches for Coupling of a Soft Robotic Sleeve to the Heart

As Published: https://doi.org/10.1007/s10439-018-2046-2

Publisher: Springer US

Persistent URL: https://hdl.handle.net/1721.1/131413

Version: Author's final manuscript: final author's manuscript post peer review, without publisher's formatting or copy editing

Towards alternative approaches for coupling of a soft robotic sleeve to the heart

Markus Horvath[1,2,4,5]*, Claudia E. Varela[1,2]*, Eimear B. Dolan[1,2,3]*, William Whyte[3-6], David S. Monahan[3], Christopher J. Payne[4,5], Isaac A. Wamala[7], Nikolay V. Vasilyev[8], Frank A. Pigula[9], David J. Mooney[4,5], Conor J. Walsh[4,5], Garry P. Duffy[3,6], Ellen T. Roche[1,2,4,510]

* Authors contributed equally to this work and are co-first authors

[1] Harvard-MIT Program in Health Sciences and Technology, Harvard Medical School, Boston, MA and Massachusetts Institute of Technology, Cambridge, MA, USA
[2] Institute for Medical Engineering Science, Massachusetts Institute of Technology, Cambridge, MA, USA
[3] Department of Anatomy, School of Medicine, College of Medicine Nursing and Health Sciences, National University of Ireland, Galway, Ireland
[4] Wyss Institute for Biologically Inspired Engineering at Harvard University, Boston, MA
[5] Harvard John A. Paulson School of Engineering and Applied Sciences, Cambridge, MA
[6]Advanced Materials and BioEngineering Research (AMBER) Centre, RCSI, NUIG & TCD, Dublin 2, Ireland
[7]The German Heart Center Berlin, Department of Cardiovascular and Thoracic Surgery, Berlin, Germany
[8] Department of Cardiac Surgery, Boston Children's Hospital, Longwood Ave, Boston, MA, USA
[9] Florida Hospital Medical Group, Orlando, Florida, USA
[10] Department of Mechanical Engineering, Massachusetts Institute of Technology, Cambridge, MA, USA

Corresponding author:

Ellen T. Roche, Massachusetts Institute of Technology, 77 Massachusetts Ave, E25-334, Cambridge, MA 02139, USA, etr@mit.edu; +1 617 2586024, Fax: 617-253-7498

Abstract

Efficient coupling of soft robotic cardiac assist devices to the external surface of the heart is crucial to augment cardiac function and represents a hurdle to translation of this technology. In this work, we compare various fixation strategies for local and global coupling of a direct cardiac compression sleeve to the heart. For basal fixation, we find that a sutured Velcro band adheres the strongest to the epicardium. Using this technique, we demonstrate that a mesh-based sleeve coupled to the myocardium further improves function in an acute porcine heart failure model. Next, we analyze the biological integration of global interface material candidates (medical mesh and silicone) in an infarcted murine model and show that a mesh interface yields superior mechanical coupling via pull-off force, histology, and microcomputed tomography. These results can inform the conception of a therapeutic approach where a mesh-based soft robotic DCC is implanted, allowed to biologically integrate with the epicardium, and actuated for active assistance at a later timepoint. This strategy may result in more efficient coupling of extracardiac sleeves to heart tissue, and lead to increased augmentation of heart function in end-stage heart failure patients.

Keywords– Direct cardiac compression, ventricular assist devices, device-tissue interface, biointegration

Introduction

Emerging soft robotic technologies are highly suited to medical applications involving human interaction due to their inherent conformability and ability to perform biomimetic motion[25]. This technology has found utility in wearable assistive devices that warrant safe, synergistic interaction with humans[21,25,29]. In addition to devices that can be worn outside the body, implantable soft robotic cardiac assist devices have recently been proposed[8,18,23,24,26,27]. We have previously reported cardiac assist devices that incorporate biomimetic actuation to emulate cardiac function in order to augment ventricular function in the failing heart[23,26,27].

The direct cardiac compression (DCC) sleeve consists of a flexible matrix material with embedded contractile actuators in a biomimetic orientation. One of the hurdles to translation of such a device is fixation to the external surface of the heart[15,27], both at mechanical anchoring points at the apex and base of the heart, and on the moving heart muscle (myocardium). As shown pre-clinically, efficient device coupling to the heart enables increased transmission of systolic assistance and twisting motion[27] while allowing for support in the diastolic or filling phase[23]. A method to achieve this coupling without septal anchoring, or excessive inflammation and injury at the epicardial surface is desirable. In this work, we compare a panel of fixation strategies for local and global coupling to the heart for their adhesion to the epicardial surface and their ability to transmit mechanical assistance, respectively. Next, we characterize interface material candidates for their host response when implanted on the epicardium, with a view to assess tissue integration for efficient coupling. Lastly, we propose a strategy for coupling our soft robotic sleeve to the heart using tissue integration; the sleeve would be implanted on the heart, subsequent native tissue integration would fixate it to the epicardium whilst providing passive restraint, and at a later time-point the sleeve would be actuated to actively augment cardiac function.

Passive restraint devices have been described to mechanically reinforce the heart and attenuate adverse remodeling of ischemic or diseased heart tissue[3]. The Acorn CorCap cardiac support device (CSD) was the first and most extensively studied passive restraint device[1]. It is composed of a flexible, polyethylene-terephthalate mesh that covers both ventricles and is designed to provide diastolic support in the longitudinal and circumferential direction. When positioned and tightened, the CSD is intended to bear enough of the end-diastolic load to reduce the degree of stretching and the magnitude of wall stress. Although this device showed promising clinical data, it was not approved by the FDA primarily over concerns of safety owing to the rate of perioperative mortality (7.8%) and durability of benefit[10,12]. Restraint level has been reported to affect the rate and degree of reverse remodeling and is an important determinant of therapy efficacy[11]. Restraint devices tested in clinical trials such as, CorCap[12] and HeartNet[5], do not allow for the measurement, adjustment or quantification of the restraint level. Lee et al.[11] demonstrate that by measuring and adjusting restraint level both at the beginning of therapy and as the heart shrinks during active reverse remodeling, restraint therapy can be optimized for improved therapeutic reverse remodeling.

Although passive restraint devices have not been clinically translated, we can learn from the results of these studies, and apply them to optimize the mechanical coupling of active devices to the heart through tissue integration. Passive restraint devices made of mesh have been reported to biologically integrate with heart tissue in pre-clinical studies[3,4,28]. In large animal heart failure models, CSD encapsulation in a highly-organized collagen network of myofibroblastic-origin has been observed 3-months post-implantation[3]. The layer of fibrous tissue produced has been shown to not accumulate with time or interfere with patent coronary arteries and veins[4,28] as well as to have similar collagen network density throughout[28]. Additionally, since no infiltrating fibrosis or inflammatory process has been evident in encapsulated CSD mesh fibers[3], tuning a biological integration approach to mechanically couple active left ventricular devices is likely a feasible alternative to current fixation methods.

Previous non-biological methods to couple active devices to the epicardium include mechanical, pneumatic and chemical fixation mechanisms[7,13,30–32]. Mechanical anchoring techniques include structural enclosure[13], a saddle-like band crossing over the upper portion of the heart between the great vessels[31], sutures through the pericardium[32] or the endocardium along the atrioventricular groove[7], and a flexible stem that extends to the abdomen[30]. Suction can also be employed on different anatomical locations on the heart[2,15,27]. Surgical adhesives have also been suggested to create a firm attachment to the epicardium[9]. However, these fixation methods have various limitations which include bulky implants, likelihood of impeding blood flow, and arrhythmogenic potential.

To evaluate the feasibility of our proposed coupling strategy, we compare the efficacy of active devices with different interface materials and fixation strategies in an acute large animal model. Next, we characterize the degree of adhesion of two of these interface materials (medical mesh and silicone) in a small animal model and measure integration histologically and by mechanical testing. These results can guide the conception of a combined therapeutic approach (Fig. 1) involving the following steps: (i) using a medical mesh material to fabricate a soft robotic sleeve, (ii) surgically implanting a passive-restraint sleeve on the heart, (iii) allowing tissue integration to couple the mesh-based sleeve to the epicardium and then (iv) initiate cardiac assistance by actuating the device. We propose that this strategy may result in more efficient coupling, and therefore increased augmentation of heart function in patients with end-stage heart failure that are waiting for a heart transplant.

Materials and Methods

Tensile strength characterization of local coupling techniques

We characterized a panel of methods for local circumferential fixation at the base of the heart: patches of gripping material (3M) assembled on a silicone band, medical mesh (Fix Pro, Bandages Plus), silicone in combination with cyano-acrylate, a custom-made strip with multiple suction elements, and Velcro (one side sutured to the heart and the other to the sleeve). For tensile testing, a freshly explanted porcine heart was mounted into a custom-made test rig, made by 3D printing and laser cutting. Steel rods were used to pierce through the heart for adequate stabilization. This assembly was fixed in the lower clamp of a mechanical tester (Instron 5566, Instron Inc.) where each test material was attached to the base of the heart and to pull-wires (1m gauge length) mounted in the upper crosshead (Fig. 2). All materials were pulled off at 100 mm/min and the maximum force was recorded for each specimen.

Acute in vivo porcine study to compare efficacy of global mechanical coupling

To compare global mechanical coupling strategies, and their effect on device performance, an acute *in vivo* pig study was conducted to test the functional efficacy of two interface materials (tough gel and medical mesh). Figure 3a-b describes the placement of the sleeve designs tested and show an image of each sleeve iteration in the unwrapped configuration. For consistency, Velcro was used for fixation at the base of the heart, and an apical suction device (Starfish® heart positioner, Medtronic) was used for fixation at the apex. Both mesh-based sleeves were fabricated using a Lycra® textile and a medical mesh (Parietex, Covidien) layer on either side. Layers were sewn together in a pre-defined pattern, thus creating inbuilt channels for subsequent insertion of pneumatic artificial muscles. The “tongue” side of a Velcro strip was sewn around the top of each device for subsequent attachment to the “groove” side which would be sutured to the base of the heart. To incorporate the suction device into the sleeve, a laser-cut acrylic ring, through which airlines from the helical actuators were placed with a clearance fit, was used. The ring was fixed around the base of the suction device, and thereby coupled to the sleeve for fixation, stabilization and transmission of torsion at the apex of the heart.

For the first sleeve design (Fig. 3a), we used a tough gel interface layer to deliberately decouple the dynamic parts of the sleeve and the myocardium thus reducing friction at the interface, as previously described[27]. In the second design (Fig. 3b), we substituted the gel liner with spots of cyano-acrylate adhesive at the device/heart interface to represent myocardial coupling between the medical mesh layer of the sleeve and the surface of the heart.

To compare coupling efficacy and device performance, an *in vivo* porcine experiment was conducted with each design (Fig. 3c). All porcine studies were realized in accordance with the Institutional Animal Care and Use Committee (IACUC) ethical and humane care guidelines at Boston’s Children’s Hospital. In brief, acute heart failure was induced to an anesthetized pig by infusing Esmolol, a short-acting cardio-selective β-blocker that reduces contractility and cardiac output. ECG, blood pressure, and blood flow were recorded at baseline (Fig. 3c-1), after cardiac output had stabilized upon

administration of Esmolol (Fig. 3c-2), and after device actuation (Fig. 3c-3). The cardiac output for each of these conditions was recorded using an ultrasonic flow probe on the aorta. Ten representative cycles were averaged and reported for each condition.

In detail, female Yorkshire swine (50-70 Kg) (n=1 per group) were used after acclimatization in holding facilities for at least a day. Animals fasted for 14-16 hours before sedation and induction of anesthesia but were not deprived of water. Swine were pre-medicated with telazol 4.5 mg/kg, xylazine 2 mg/kg, and atropine 0.04 mg/kg, delivered intramuscularly. Animals were anesthetized, intubated, and placed on mechanical ventilation using volume-cycled ventilation at 10 mL/kg at 10-20 breaths/min. Anesthesia was maintained with isoflurane (0.5-1%) and oxygen. When the animals were stabilized, a femoral venous and arterial line were placed percutaneously followed by introduction of a jugular catheter (Veterinary Central Venous Catheter Set, Ref CVS50IJ, Surgivet). Lidocaine was administered prophylactically to reduce the risk of arrhythmias caused by the placement and attachment of each device. A bolus intravenous (IV) injection dose (0.5-1.5 mg/kg) was administered at ~25–50 mg/min. An IV infusion at 20–50 mcg/kg/min was then administered followed by an additional bolus dose of 0.5–0.75 mg/kg at 5-10 minute intervals as necessary, up to a total dose of 3 mg/kg. Unfractionated Heparin (300iu/Kg IV) was administered prophylactically to reduce the risk of venous thromboembolism during the procedure. The heart was exposed via a sternotomy. A paralytic agent (Cisatrocurium, 0.1-0.4mg/kg IV) was administered to facilitate sternotomy and avoid excessive muscular fasciculations. The animal was instrumented with an ultrasonic flow probe on the aorta and pulmonary trunk (16PS and 20PS, Transonics Inc.) connected to a T402 multi-channel research console (Transonics Inc.). The left atrium and pulmonary artery were cannulated with 26G catheters and a pressure sensor (Surgivet Inc.) was attached to each catheter. Continuous monitoring during the procedure included ECG tracings, arterial blood pressure, and central venous blood pressure through femoral lines, intra-ventricular pressures, pulmonary and aortic flow rates and SpO_2 level. ECG and pressure data were logged to a data acquisition system via a 9-pin analog connector from a Surgivet vital signs monitor (Surgivet). Flow data was logged using a Powerlab data acquisition module and LabChart software (AD instruments). After instrumentation and establishment of a stable hemodynamic condition, 5 min of baseline data were recorded to measure cardiac performance. Epicardial pacing was used to control the heart rate, if necessary, to help with device synchronization. Acute heart failure was pharmacologically induced using Esmolol. Effects were seen within 2 min and peaked at around 5 min, lasting up to about 10 min. Up to 5 boluses of Esmolol for a total of 0.1-1.0 mg/kg, and a constant rate of infusion (CRI) of 0.1-2.0 mg/kg/min were delivered to allow a stable acute heart failure model for a period of about 1 hr. With the induction of this model, heart rate (and as a result cardiac output) decreases. Each device was placed on the heart and affixed using the active suction cup at the apex, and Velcro at the base. Cyanoacrylate adhesive was applied for the “coupled” design.

The DCC devices were actuated using a control box that supplies pressurized air to the contracting actuators, triggered by a pacemaker signal while the heart was being paced. Heart rate and device rate were manually fine-tuned by the surgeon with a dual chamber pacemaker (5342, Medtronic Inc.). Air pressure regulators (ITV series, SMC

Corporation) were used to set the actuation pressure and a bank of 16 pneumatic valves (high-flow 3-way VQ series, SMC corporation) enables independent actuation of each actuator. The device was synchronized using a pacemaker signal which is acquired by a data acquisition system (X-Series DAQ card, National Instruments) and a PC was used to control the pneumatic valves. A vacuum source provided a means of relaxing the actuators during the diastolic phase of the cardiac cycle.

At the end of the trial (maximum length four hours), the animal was euthanized by an intra-venous injection of Fatal Plus (110mg/kg).

Material characterization of medical mesh and silicone

Medical grade silicone (Shore 00-40, Med-4901, NuSil Technology LLC), silicone that had been used for previous work (Dragon Skin FX-Pro, Smooth-on Inc.) and medical mesh (Parietex, Covidien) were selected as potential interface materials for material evaluation, with Nusil and medical mesh being suitable for subsequent chronic *in vivo* implantation. 1.3mm (Med-4901) or 3mm (Dragon Skin FX-Pro) thick silicone dogbone specimens were cast in a 3D-printed mold to the recommended dimensions in ASTM D412 for elastomers and medical mesh was sized according to ASTM D5035 for fabrics without altering its thickness. Samples of either medical mesh or silicone were tested in a universal testing machine (Instron 5944, Instron Inc.). Specimens were cyclically tested to 60% of the material's ultimate tensile strength (n=1 specimen for 20 cycles) and creep tested (n=5) by holding the force at 60% of the material's ultimate tensile strength for 15 minutes. Specimens were tensile tested to failure (n=5) according to ASTM D412 and ASTM D 5035.

In vivo study to compare medical mesh and silicone tissue integration

To evaluate tissue integration of the selected interface materials, an *in vivo* murine study was performed (Fig. 4). 3 x 3 mm square patches of medical mesh (Parietex, Covidien) or silicone were used for surgical implantation at the epicardial surface. Prior to the procedure, 300 µm thick medically approved silicone sheets (Shore 00-40, Med-4901, NuSil Technology LLC) were cast using a film applicator (Elcometer 4340, Elcometer Inc.), then both silicone and mesh patches were cut to size using a laser cutter (VLS2.30, Universal Laser System), and sterilized by autoclave.

All animal studies were carried out in the Brigham and Women's Hospital Rodent Cardiovascular Physiology Core and in accordance with their IACUC ethical and humane care guidelines.Medical mesh or silicone patches were implanted in ten male C57 mice (22-31 g, Jackson Laboratories) which were either healthy or had a myocardial infarction (MI) (n=7 MI, n=3 healthy). In detail, mice were anesthetized with isoflurane (1-3% isoflurane in oxygen) in an anesthetizing chamber. Chest hair was removed with hair removal cream and pre-operative buprenorphine (0.05 mg/kg subcutaneously) was administered. The animal was then intubated, connected to a mechanical ventilator, and placed on a sterile drape over a heating pad for the duration of the surgery. A thoracotomy was performed to expose the heart and the pericardium was removed using fine forceps. To generate a myocardial infarction (n=7 per material group), an 8-0 prolene suture was used to permanently ligate the left anterior descending coronary artery (LAD) approximately one third of the way from the apex to

the base of the heart. Myocardial blanching after LAD ligation was apparent confirming infarction. In all animals, a suture (8-0 prolene) was placed on the upper right corner and lower left corner of the patch to secure patch placement. In infarcted animals, patches were attached between the coronary ligation site and the apex of the heart and included both infarcted and non-infarcted tissue. Placement was replicated in healthy animals. The thoracotomy incision was closed with 4-5 interrupted sutures (5-0 polysorb). After removal of anesthesia, animal was ventilated with 100% oxygen on a heated pad. When autonomous breathing was recovered, the intubation catheter was removed. 50 µl of buprenorphine (0.05 mg/kg) were given IP every 12h for 3 days post-operatively. Animals were euthanized by IP pentobarbital (100µL/mouse at 50 mg/ml) injection. Hearts were excised, flushed with phosphate buffered saline, weighed and either kept in saline at 4°C until use or fixed with 10% formalin for 24 hours.

Pull-off testing of integrated medical mesh and silicone patches

Fresh mouse hearts with integrated epicardial materials were mounted onto a custom-made fixation rig held by the lower, stationary grips of a tensile testing machine (Instron 5566, Instron Inc.). A modified crocodile clip connected to the upper clamps of the tensile tester by flexible wire was used to grip the material on the surface of the heart. After epicardial patch was gripped, sutures holding the patch in place were removed using micro-scissors. The integrated material was detached from the epicardium in shear at a rate of 20 mm/min. The maximum tangential adhesion force was recorded.

Microcomputed tomography imaging of whole heart samples

To enhance tissue contrast, fresh mouse hearts were stained with Potassium Iodide (KI) vapor prior to imaging. Briefly, each heart was dried using KimWipes and suspended in a glass bottle containing 500 mg of KI (Sigma). Glass bottles were sealed air tight and left at room temperature for either 24 h (medical mesh sample) or 72 h (silicone sample). For image data collection, samples were inserted in a polypropylene tube (7.5 mm diameter) with Styrofoam and placed into a XRA-002 X-Tek µCT system. The 3D reconstructions were performed using CT-Pro (Nikon Metrology) and the surface renderings were generated using VGStudio Max. Transverse and longitudinal 2D views of each model were used to evaluate material-tissue conformability.

Histology and fibrous capsule thickness

After fixation, whole rodent hearts underwent tissue processing and were embedded in paraffin wax. Subsequently, 5µm sections were cut, mounted onto glass slides, and stained using standard Haematoxylin and Eosin or Masson trichrome stain. Images were then taken using a virtual slide microscope (Olympus VS120) and viewed using Olympus software (OlyVIA Ver2.9). Fibrous capsule thickness at the inner surface (i.e. in contact with the epicardium) and outer surface (i.e. not in contact with the epicardium) of material patches was individually measured using ImageJ.

Statistical Analysis

A one-way analysis of variance (ANOVA) with a Dunnett's multiple comparison test, (where the Velcro group was compared to all other groups) was performed for the adhesion study. A one-way ANOVA with a Tukey's multiple comparison post-hoc test

was performed for the *in vivo* porcine studies. Every group was compared to each other. For comparison of host response thickness, a one-way ANOVA with Sidak's multiple comparison post-hoc test was used. The integrated tissue/mesh thickness was compared to the total fibrous capsule thickness for the silicone groups with and without MI. A confidence interval of 95% was used for all ANOVA tests. No statistical analysis was carried out for the mechanical testing as we were limited to n=1 per group.

Results

Tensile strength characterization of local coupling techniques

From the panel of basal fixation techniques evaluated, the strongest adhesion to fresh heart tissue was with Velcro at 54±8.9N (Fig.5). An adhesion force of up to 15N was recorded for cyano-acrylate adhesive with either mesh or silicone at the heart/tissue interface. Based on these results, Velcro was used for acute *in vivo* porcine testing to ensure reliable local coupling and facilitate global coupling evaluation.

Acute in vivo porcine study to compare efficacy of global mechanical coupling

The decoupled sleeve with the gel at the heart/device interface restored cardiac output to baseline (Fig. 6a) in an acute heart failure porcine model. The coupled sleeve, however, was able to increase cardiac output above baseline (Fig. 6b), while also having the potential to increase diastolic function, as previously described[1].

Material characterization of medical mesh and silicone

Stress-strain analysis materials showed a higher ultimate tensile strength of the Dragon Skin FX-Pro material (1.73±0.19 MPa, n=5) compared to the MED-4901 (1.11±0.17 MPa, n=5) and Parietex medical mesh (1.14±0.11 MPa, n=5). The mesh material was stiffer and failed at a lower strain value (Fig 7a). Cyclical testing to 20 cycles showed hysteresis, more significant in the Dragon Skin FX-Pro compared to the other two materials (Fig 7b). Creep was highest for the most viscoelastic materials, Dragon Skin FX-Pro (Fig 7c).

In vivo study to compare medical mesh and silicone tissue integration

Microcomputed tomography imaging of whole heart samples

Surface renderings obtained from µCT imaging were used to evaluate conformability of medical mesh and silicone to heart tissue 4-7 days post-MI. No separation between the implanted mesh material and the heart tissue was observed through all transverse slices of the corresponding model. Indeed, some integration between the mesh and heart tissue was evident (Fig. 7d, left). On the contrary, areas of separation between the silicone and epicardial surface were present and no integration to the tissue was observed (Fig. 7d, right). Overall, at an acute timepoint post-MI, the medical mesh shows conformability to the epicardial surface and early signs of tissue integration.

Pull-off testing of medical mesh and silicone specimens at acute and chronic time points

The tangential adhesion force of epicardial materials to the heart was recorded as a measurement of tissue integration using a pull-off test set-up (Fig 7e). Results show a greater integration of tissue into medical mesh compared to silicone in both MI (Fig. f)

and healthy hearts (Fig. 7g). Both materials showed greater integration in MI hearts compared to healthy hearts. Maximal adhesion strength was achieved 14d after mesh implantation on an infarcted heart (2.27 N), followed by the 14d mesh implant on healthy tissue (0.91N). In contrast, at 14d post-implantation, silicone adhesion strength to infarcted tissue was 0.1N. Although the pull-off force of both materials at the chronic time-point is higher than the 4d pull-off for each (0.1N and 0.05N respectively), a more pronounced change over time was observed for the specimens with mesh implants, indicating increased tissue integration between 4d and 14d.

Histology and fibrous capsule thickness

Representative results from histological analysis are shown in Fig. 8. Strikingly different host responses to the silicone and medical mesh implants are demonstrated by H&E staining (Fig. 8a) and Masson's Trichrome (Fig. 8b). As the silicone is impervious to cell ingrowth, a fibrous capsule (FC) grows around the implant (Fig. 8a,b). In contrast, the mesh allows fibrous tissue ingrowth in between the mesh pores and integrates the implant with heart tissue allowing for better mechanical coupling which is important for this application. The granulation tissue was significantly thicker than the combined thickness of the fibrous capsule (inner and outer) as shown in Fig. 8c. Overall, a standard foreign body response was noted with both materials with the main difference being that the silicone patch became encapsulated whereas the native tissue interdigitated between the mesh pores, thereby coupling it to the heart tissue. The components of the response were granulation tissue with chronic inflammatory cells, vascularization, collagen and fibroblasts. There were no signs of necrosis, infection, or toxic leaching. For this application, the most important aspect is the mechanical coupling of the implant to the tissue, which is superior for the mesh implant.

Discussion

We have compared a panel of methods for attaching a soft active sleeve to the heart surface, both at the base of the heart and on the moving heart muscle. First, we compared fixation methods for the base of the heart (including suction, gripping material, adhesive) and found that a velcro/suture combination is the most effective. Next, we assessed whether coupling to the myocardium is beneficial to the performance of an active cardiac assist device. We created a mesh-based active sleeve and demonstrated that it can augment cardiac output in an acutely failing porcine heart. We showed that global coupling of the sleeve to the myocardium with adhesive further augments cardiac output as compared to when the sleeve is deliberately decoupled from the moving heart muscle using a gel liner. Motivated by the finding that global myocardial coupling augments device performance and armed with the knowledge that adhesives may not be strong and flexible enough to achieve this coupling, we then explored the idea of using the host response to integrate a mesh-based sleeve into the myocardium. To this end, we compared two materials for their elicited host responses when epicardially implanted on healthy and infarcted rat hearts in terms of (i) histological response (ii) conformability and (iii) pull-off strength. We showed that a medical mesh implant integrates with the epicardial tissue more substantially than a silicone implant. Fibrotic tissue enshrouded the mesh fibers, efficiently coupling the mesh patch to the epicardium as shown by a higher pull-off strength and increased

conformability. In contrast, a fibrotic capsule was formed around the silicone patch as native cells were not able to penetrate the material, thus impacting adhesion strength and yielding inferior coupling.

The results of this study suggest that exploiting the host response of an epicardially placed soft robotic sleeve could be advantageous in terms of mechanically coupling it to the myocardium. The approach would be as follows; a sleeve fabricated from medical mesh is surgically implanted onto the epicardium, but not activated immediately to allow for integration into host tissue while acting as a ventricular restraint device for this period. Following tissue integration, the coupled sleeve is actuated to actively augment cardiac function. Using biointegration as a coupling strategy could improve device performance by allowing diastolic assistance, and superior transmission of twisting motion[27].

There are several avenues that warrant further exploration to drive this idea down the path of clinical translation. First, the degree of biointegration is likely a function of scaffold pore size[19]. For any scaffold and cell type combination, a critical range of pore sizes exists[16,17,20]. The pores must be small enough to establish a sufficiently high specific surface area for efficient binding of a critical number of cells but also need to be sufficiently large to allow for cell migration[22]. Thus, tuning the degree of mesh integration with the epicardium could be done by optimizing the pore size of the mesh and the ligands present at the surface of the material. Second, by placing the mesh only over the infarcted region the mesh will potentially integrate selectively with the diseased tissue, and not the surrounding heathy tissue. In this fashion, the sleeve could be tailored to match the disease severity of the patient. Third, the idea that the passive sleeve could provide ventricular restraint before being activated could be beneficial to the overall therapeutic strategy and should be investigated further. Previous whole heart passive restraint devices have shown promising preliminary clinical data[10,12]. Computational modeling has suggested that ventricular restraint can significantly reduce end-diastolic myofiber stress without negatively impacting pump function, especially when localized to the LV, and so a tailored mesh-based sleeve whereby additional support is provided to selective areas could be beneficial[33,14].

The major limitation we encountered is a high mortality rate up to 7 days post-MI during our murine study; likely because the implanted patches imposed a significant load on the infarcted region of the murine heart leading to ventricular rupture. However, a larger animal model may tolerate post-infarct epicardially placed implants better than mice[6,22]. Additionally, multiple survival surgeries would allow for patch implantation to occur at a later time-point and not at the time of MI creation, more closely representing our proposed therapeutic strategy.

The deductions that can be drawn from our study are as follows; (i) medical mesh material can be used to fabricate an active heart sleeve that can increase cardiac output on a failing heart, (ii) coupling a mesh-based sleeve to the myocardium can impart greater functional improvement than a decoupled sleeve, (iii) biointegration can be used to couple the mesh material with the myocardium. Future studies will optimize the time and degree of biointegration before actuating the integrated sleeve. This strategy could

result in more efficient coupling to improve the performance of the device and thereby increase augmentation of heart function in patients with end-stage heart failure.

Acknowledgments

The authors would like to thank Ronghli Liao PhD, Sudeshna Fisch PhD, and Souen Ngoy from the Brigham and Women's Hospital Rodent Cardiovascular Physiology Core for their technical support; the staff at ARCH, Boston Children's Hospital for help with porcine studies, James Weaver PhD, Wyss Institute at Harvard University for imaging assistance and Robert Padera MD PhD for histological assessment. ETR acknowledges funding from the Massachusetts Institute of Technology, (Institute for Medical Engineering Science and the Department of Mechanical Engineering), The Wyss Institute for Biologically Inspired Engineering at Harvard University. WW and GD acknowledge the Irish Research Council (GOIPG/2017/927) and Science Foundation Ireland (SFI/12/RC/2278).

REFERENCES

1. Alferness, C. U.S. Pat. No. 5,702,343 Cardiac reinforcement device. , 1996.
2. Anstadt, M., R. Bartlett, J. Malone, G. Brown, S. Martin, D. Nolan, K. Oberheu, and A. GL. Direct mechanical ventricular actuation for cardiac arrest in humans. A clinical feasibility trial. *Chest* 100:86–92, 1991.
3. Blom, A. S., R. Mukherjee, J. J. Pilla, A. S. Lowry, W. M. Yarbrough, J. T. Mingoia, J. W. Hendrick, R. E. Stroud, J. E. McLean, J. Affuso, R. C. Gorman, J. H. Gorman, M. A. Acker, and F. G. Spinale. Cardiac Support Device Modifies Left Ventricular Geometry and Myocardial Structure After Myocardial Infarction. *Circulation* 112:1274 LP-1283, 2005.
4. Chaudhry, P. A., P. V Anagnostopouls, T. Mishima, G. Suzuki, H. Nair, H. Morita, V. G. Sharov, C. Alferness, and H. N. Sabbah. Acute ventricular reduction with the acorn cardiac support device: effect on progressive left ventricular dysfunction and dilation in dogs with chronic heart failure. *J. Card. Surg.* 16:118–126, 2001.
5. Costanzo, M. R., S. Maybaum, A. Bank, I. Anand, B. Rayburn, R. Ivanhoe, and W. Abraham. Ventricular Elastic Support Therapy (VEST) in Stage C Heart Failure-Analysis from the PEERLESS-HF Study. *J. Card. Fail.* 16:912, 2010.
6. Fujimoto, K. L., K. Tobita, W. D. Merryman, J. Guan, N. Momoi, D. B. Stolz, M. S. Sacks, B. B. Keller, and W. R. Wagner. An Elastic, Biodegradable Cardiac Patch Induces Contractile Smooth Muscle and Improves Cardiac Remodeling and Function in Subacute Myocardial Infarction. *J. Am. Coll. Cardiol.* 49:2292–2300, 2007.
7. Ghanta, R. K., L. S. Lee, R. Umakanthan, R. G. Laurence, J. a. Fox, R. M. Bolman, L. H. Cohn, and F. Y. Chen. Real-time adjustment of ventricular restraint therapy in heart failure. *Eur. J. Cardio-thoracic Surg.* 34:1136–1140, 2008.
8. Horvath, M. A., I. Wamala, E. Rytkin, E. Doyle, C. J. Payne, T. Thalhofer, I. Berra, A. Solovyeva, M. Saeed, S. Hendren, E. T. Roche, P. J. del Nido, C. J. Walsh, and N. V Vasilyev. An Intracardiac Soft Robotic Device for Augmentation of Blood Ejection from the Failing Right Ventricle. *Ann. Biomed. Eng.* 45:2222–2233, 2017.
9. Kung, R. T., and M. Rosenberg. Heart booster: a pericardial support device. *Ann. Thorac. Surg.* 68:764–7, 1999.
10. Kwon, M. H., M. Cevasco, J. D. Schmitto, and F. Y. Chen. Ventricular restraint therapy for heart failure: A review, summary of state of the art, and future directions. *J Thorac Cardiovasc Surg* 144:771–777.e1, 2012.
11. Lee, L. S., R. K. Ghanta, S. A. Mokashi, O. Coelho-Filho, R. Y. Kwong, M. Kwon, J. Guan, R. Liao, and F. Y. Chen. Optimized ventricular restraint therapy: adjustable restraint is superior to standard restraint in an ovine model of ischemic cardiomyopathy. *J Thorac Cardiovasc Surg* 145:824–831, 2013.
12. Mann, D. L., S. H. Kubo, H. N. Sabbah, R. C. Starling, M. Jessup, J. K. Oh, and M. A. Acker. Beneficial effects of the CorCap cardiac support device: five-year results from the Acorn Trial. *J Thorac Cardiovasc Surg* 143:1036–1042, 2012.
13. Meister, M., and S. M. Wildhirt. Cardiac Assistance Device and Method for the Control thereof. Patent: US8944987B2, 2015.
14. Mokashi, S. A., L. S. Lee, J. D. Schmitto, R. K. Ghanta, S. McGurk, R. G. Laurence, R. M. Bolman, L. H. Cohn, and F. Y. Chen. Restraint to the left ventricle alone is superior to standard restraint. *J. Thorac. Cardiovasc. Surg.*

146:192–197, 2013.
15. Moreno, M. R., S. Biswas, L. D. Harrison, G. Pernelle, M. W. Miller, T. W. Fossum, D. a. Nelson, and J. C. Criscione. Development of a Non-Blood Contacting Cardiac Assist and Support Device: An In Vivo Proof of Concept Study. *J. Med. Device.* 5:41007-1-41007–9, 2011.
16. Murphy, C. M., M. G. Haugh, and F. J. O'Brien. The effect of mean pore size on cell attachment, proliferation and migration in collagen-glycosaminoglycan scaffolds for bone tissue engineering. *Biomaterials* 31:461–466, 2010.
17. Murphy, C. M., and F. J. O'Brien. Understanding the effect of mean pore size on cell activity in collagen-glycosaminoglycan scaffolds. *Cell Adh. Migr.* 4:377–381, 2010.
18. Mac Murray, B. C., C. C. Futran, J. Lee, K. W. O'Brien, A. A. Amiri Moghadam, B. Mosadegh, M. N. Silberstein, J. K. Min, and R. F. Shepherd. Compliant Buckled Foam Actuators and Application in Patient-Specific Direct Cardiac Compression. *Soft Robot.* , 2017.
19. O'Brien, F. J. Biomaterials & scaffolds for tissue engineering. *Mater. Today* 14:88–95, 2011.
20. O'Brien, F. J., B. A. Harley, I. V Yannas, and L. J. Gibson. The effect of pore size on cell adhesion in collagen-GAG scaffolds. *Biomaterials* 26:433–441, 2005.
21. O'Neill, C. T., N. S. Phipps, L. Cappello, S. Paganoni, and C. J. Walsh. A soft wearable robot for the shoulder: Design, characterization, and preliminary testing. , 2017.
22. Park, J., S. Choi, A. H. Janardhan, S.-Y. Lee, S. Raut, J. Soares, K. Shin, S. Yang, C. Lee, and K.-W. Kang. Electromechanical cardioplasty using a wrapped elasto-conductive epicardial mesh. *Sci. Transl. Med.* 8:344ra86-344ra86, 2016.
23. Payne, C. J., I. Wamala, C. Abah, T. Thalhofer, M. Saeed, D. Bautista-Salinas, M. A. Horvath, N. V Vasilyev, E. T. Roche, F. A. Pigula, and C. J. Walsh. An Implantable Extracardiac Soft Robotic Device for the Failing Heart: Mechanical Coupling and Synchronization. *Soft Robot.* , 2017.doi:10.1089/soro.2016.0076
24. Payne, C. J., I. Wamala, D. Bautista-Salinas, M. Saeed, D. Van Story, T. Thalhofer, M. A. Horvath, C. Abah, J. Pedro, and C. J. Walsh. Soft robotic ventricular assist device with septal bracing for therapy of heart failure. *Sci. Robot.* 2:eaan6736, 2017.
25. Polygerinos, P., N. Correll, S. A. Morin, B. Mosadegh, C. D. Onal, K. Petersen, M. Cianchetti, M. T. Tolley, and R. F. Shepherd. Soft Robotics: Review of Fluid- Driven Intrinsically Soft Devices; Manufacturing, Sensing, Control, and Applications in Human- Robot Interaction. *Adv. Eng. Mater.* , 2017.
26. Roche, E. T., M. A. Horvath, A. Alazmani, K. C. Galloway, N. V Vasilyev, D. J. Mooney, F. A. Pigula, and C. J. Walsh. Design and fabrication of a soft robotic direct cardiac assist device. , 2015.
27. Roche, E. T., M. A. Horvath, I. Wamala, S. E. Song, W. Whyte, Z. Machaidze, N. V Vasilyev, D. J. Mooney, F. A. Pigula, and C. J. Walsh. Soft Robotic Sleeve Restores Heart Function. *Sci. Transl. Med.* 9:eaaf3925, 2017.
28. Sabbah, H. N., V. G. Sharov, P. A. Chaudhry, G. Suzuki, A. Todor, and H. Morita. Chronic therapy with the acorn cardiac support device in dogs with chronic heart failure: three and six months hemodynamic, histologic and ultrastructural findings.

J. Heart Lung Transplant. 20:189, 2001.
29. Sasaki, D., T. Noritsugu, and M. Takaiwa. Development of active support splint driven by pneumatic soft actuator (ASSIST). , 2005.
30. Shahinpoor, M., and K. J. Kim. Design , Development and Testing of A Multi-Fingered Heart Compression / Assist Device Equipped with IPMC Artificial Muscles. 4329:411–420, 2001.
31. Smith, E. M. Cardiac massage apparatus. , 1962.
32. Trumble, D. R., C. S. Park, and J. A. Magovern. Copulsation Balloon for Right Ventricular Assistance: Preliminary Trials. , 2015.
33. Wenk, J. F., L. Ge, Z. Zhang, D. Mojsejenko, D. D. Potter, E. E. Tseng, J. M. Guccione, and M. B. Ratcliffe. Biventricular Finite Element Modeling of the Acorn CorCap Cardiac Support Device on a Failing Heart. *Ann. Thorac. Surg.* 95:2022–2027, 2018.
34. Yannas, I. V, E. Lee, D. P. Orgill, E. M. Skrabut, and G. F. Murphy. Synthesis and characterization of a model extracellular matrix that induces partial regeneration of adult mammalian skin. *Proc. Natl. Acad. Sci.* 86:933–937, 1989.

Figures and captions

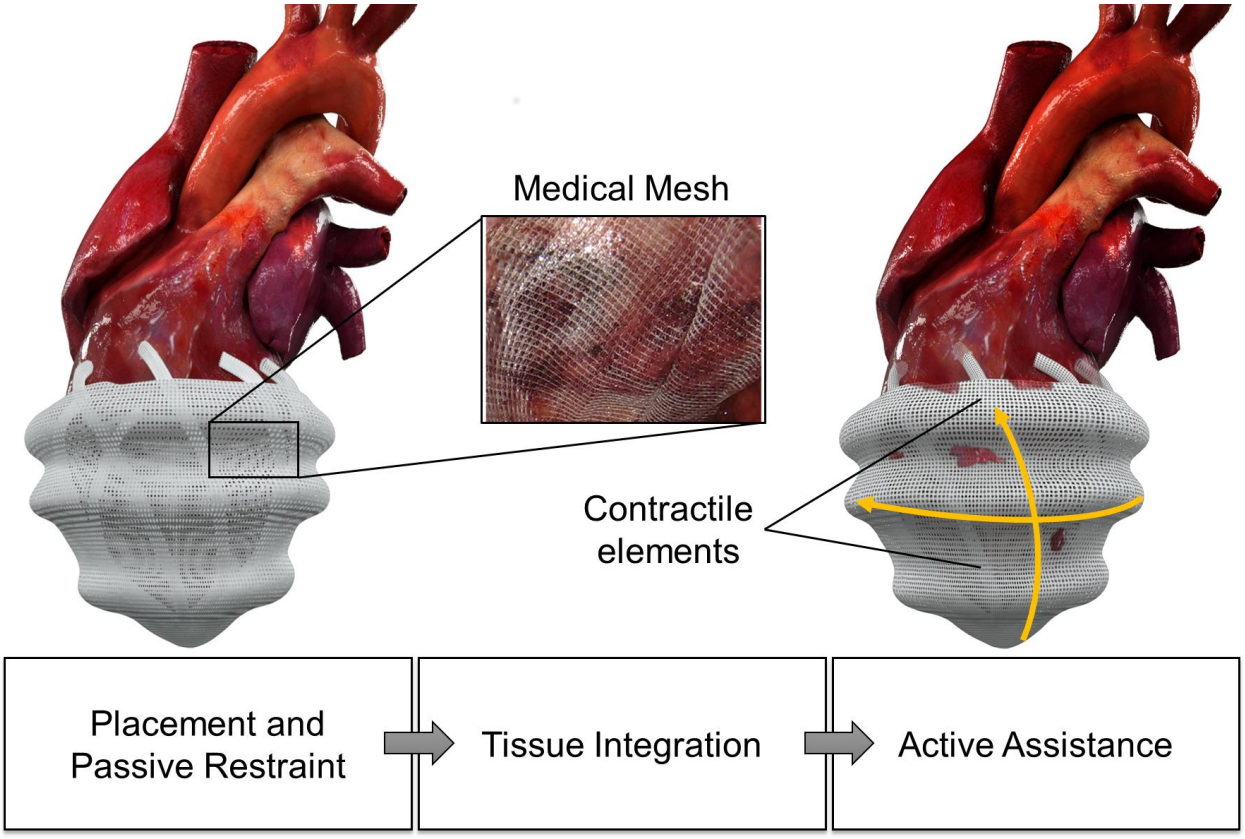

Figure 1: An overview of the proposed therapeutic strategy. A passive robotic sleeve is placed around the heart, allowed to integrate with the tissue, and then actuated to provide active assistance.

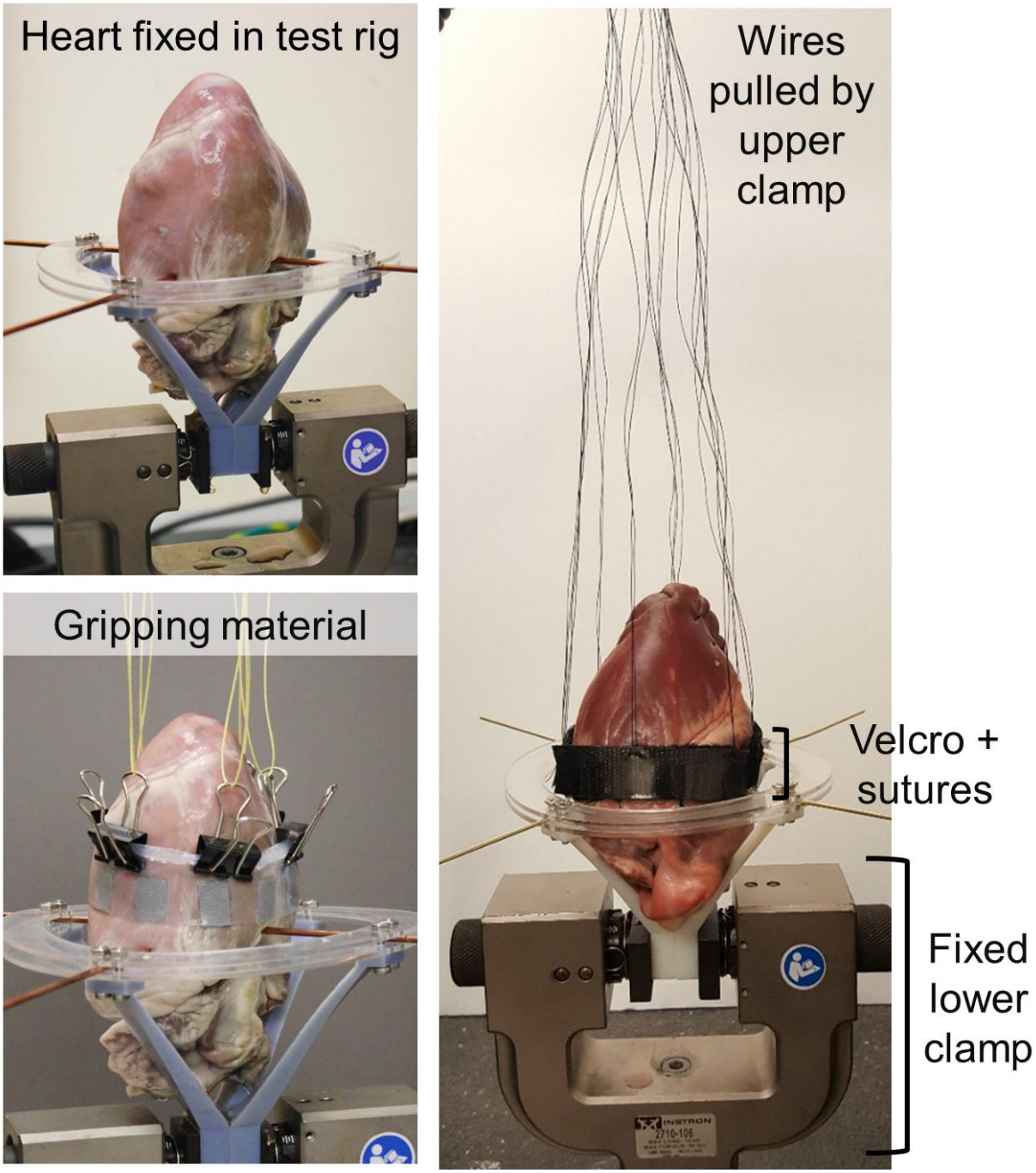

Figure 2: Test set up for basal fixation testing. A test-rig was custom designed to fix the heart to the lower clamp of a mechanical tester. Each specimen was attached to the heart and pulled off using pull-wires with the moving upper clamp. Set up is shown for the gripping material (left) and for Velcro (right), figure adapted from [27].

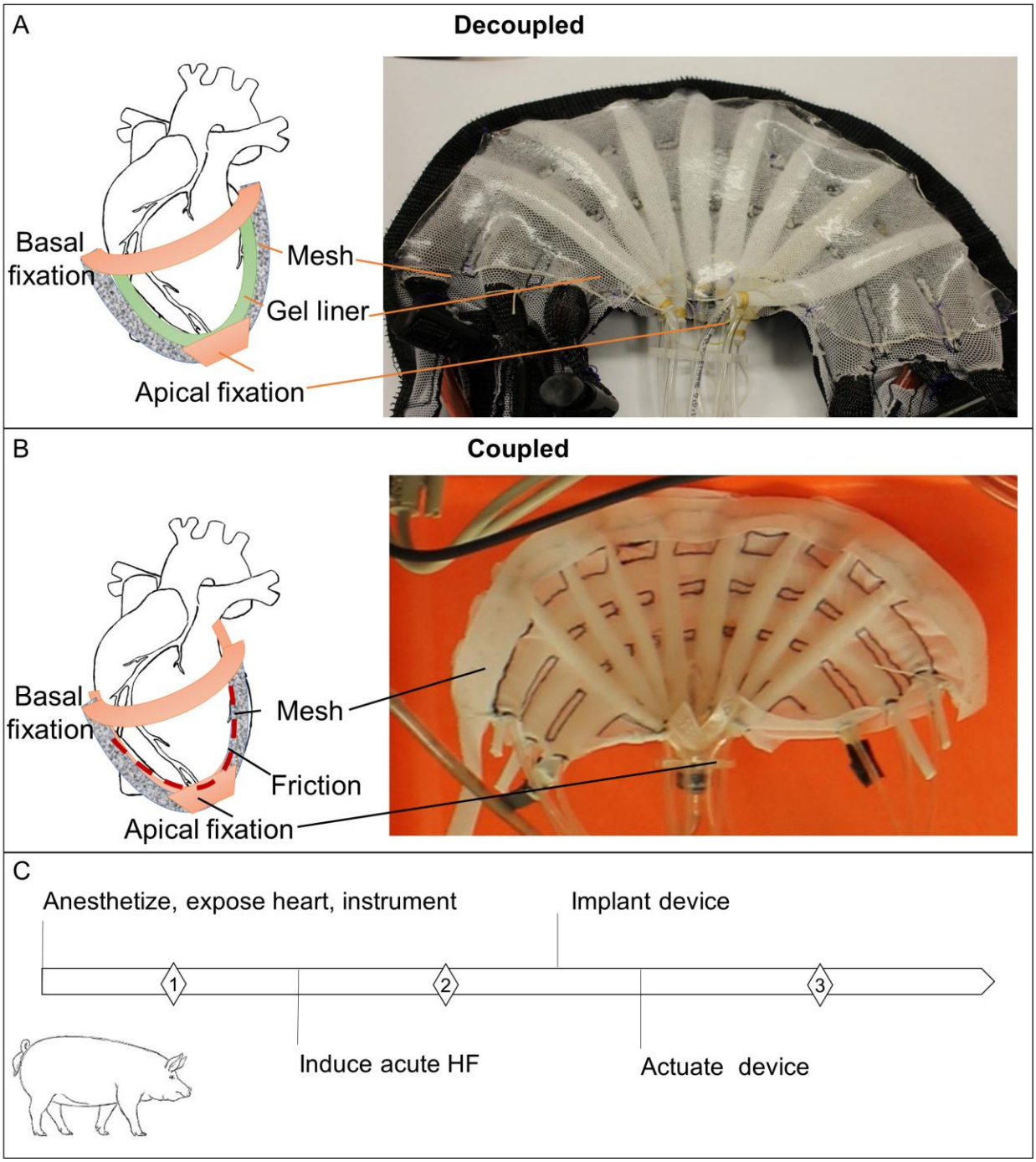

Figure 3: Acute *in vivo* porcine study description. A)"Decoupled" device – a mesh-based device with a "tough gel" liner between the heart and device was used. B) "Coupled" device – a mesh-based device with cyano-acrylate adhesive to allow coupling to the heart. C) Acute study overview. The heart was exposed and data collected [1], heart failure was induced with Esmolol, data was collected [2], then device was implanted, actuated and data was collected [3].

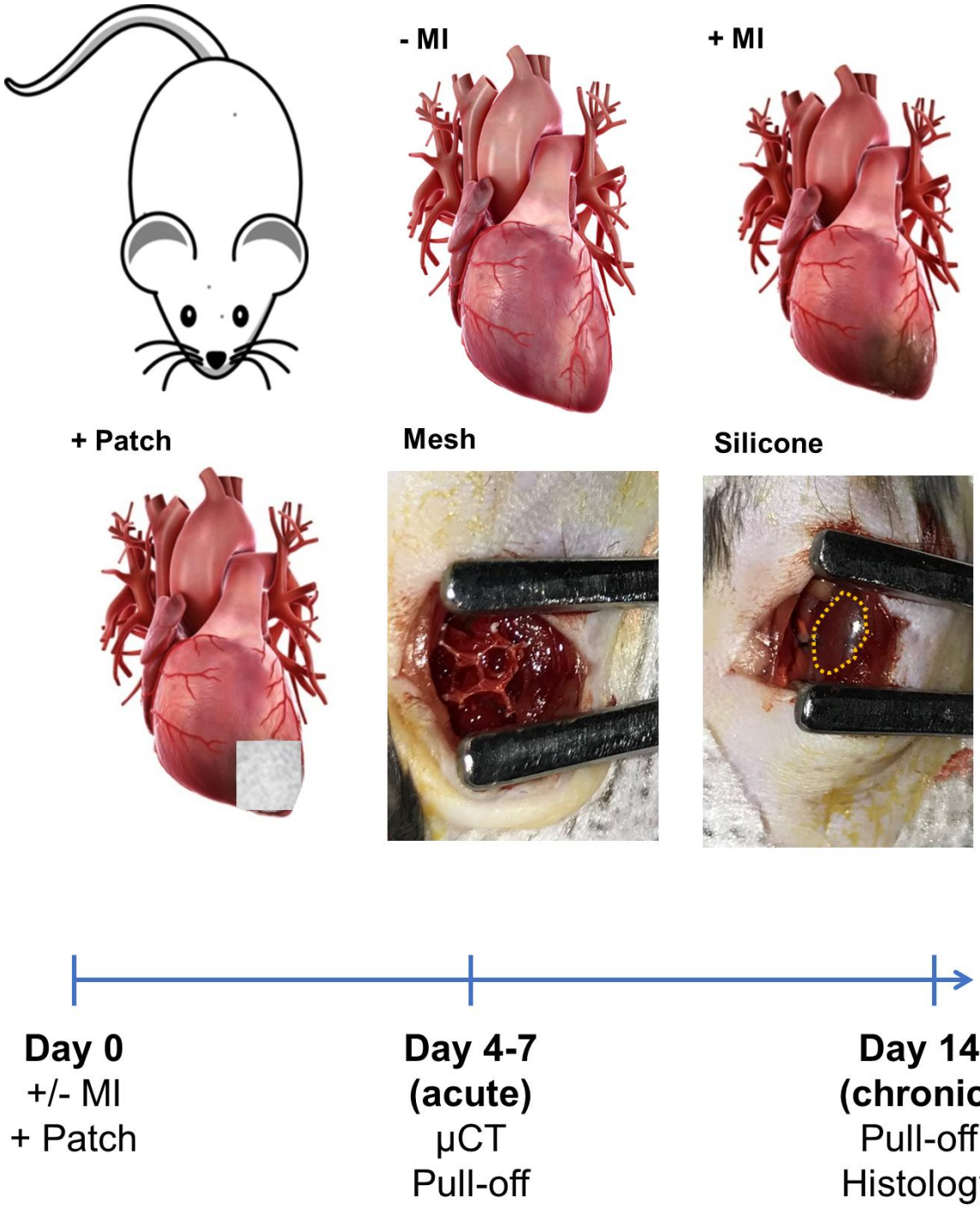

Figure 4: *In vivo* murine study set-up. Groups were +/- MI with either silicone or mesh patches. Infarct was created at day 0, then patch was implanted. µCT imaging (n=1) and pull-off testing (n=1) were conducted at an acute time-point (days 4-7). At day 14, pull-off (n=1) and histology (n=2) was carried out for evaluation of chronic tissue integration.

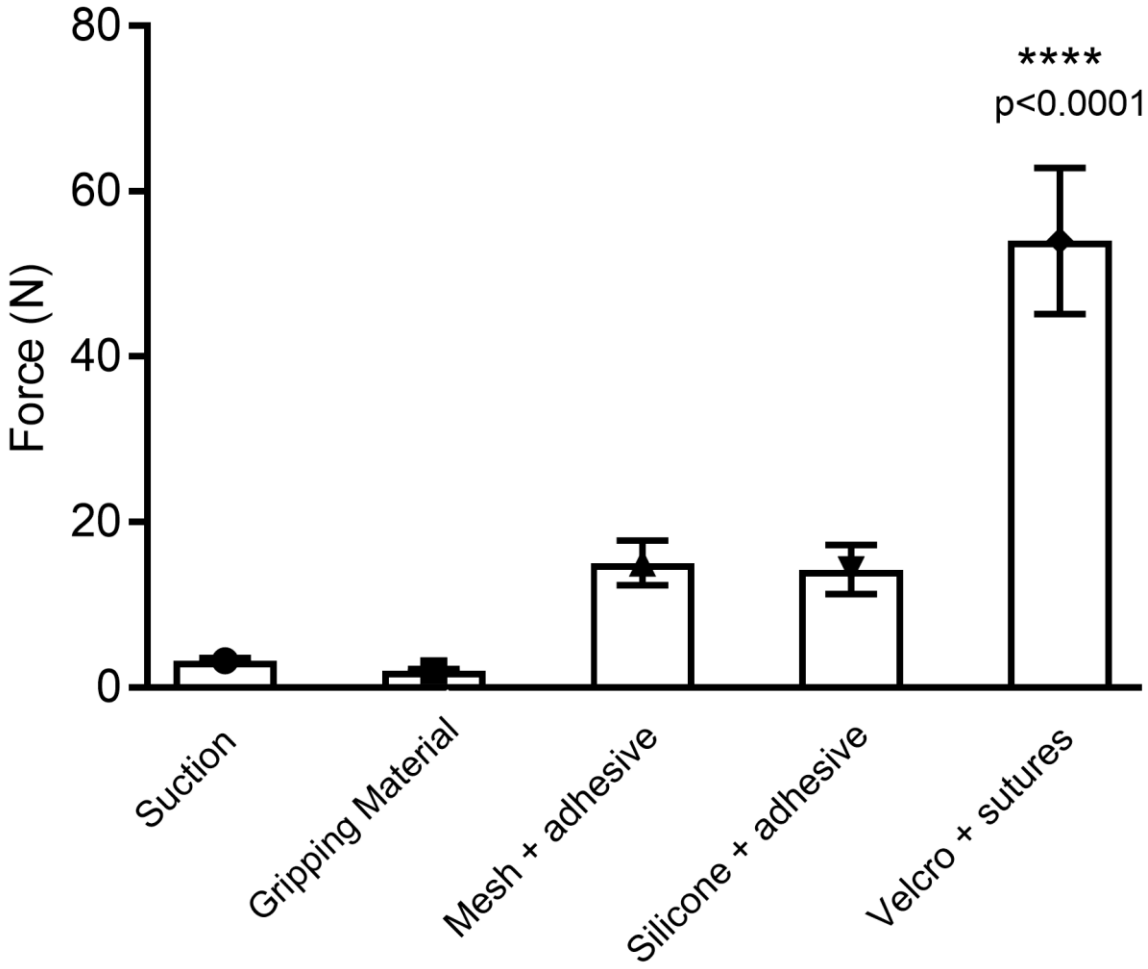

Figure 5: Pull-off force for basal fixation methods. The Velcro pull-off force was significantly different to each of the other groups, using a one-way ANOVA with Dunnett's multiple comparisons test where all values were compared to Velcro, ****p<0.0001 , values are mean ± standard deviation, n=3.

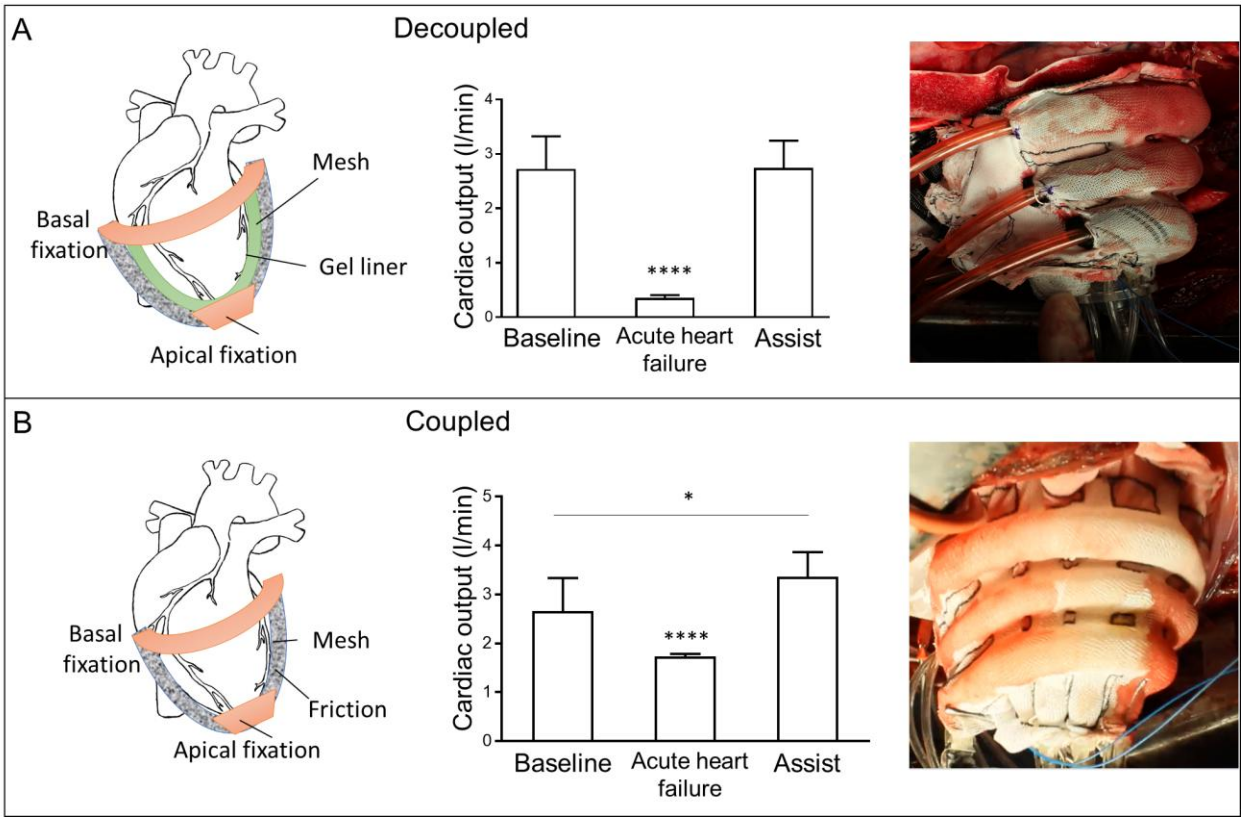

Figure 6: Acute *in vivo* porcine study results. A) The decoupled device restored cardiac output to baseline once device was actuated. B) The coupled device restored cardiac output above baseline. A one-way ANOVA with Tukey's multiple comparisons was used. ****p<0.0001. *p<0.05, data are shown as mean + standard deviation, n=10 consecutive representative cycles.

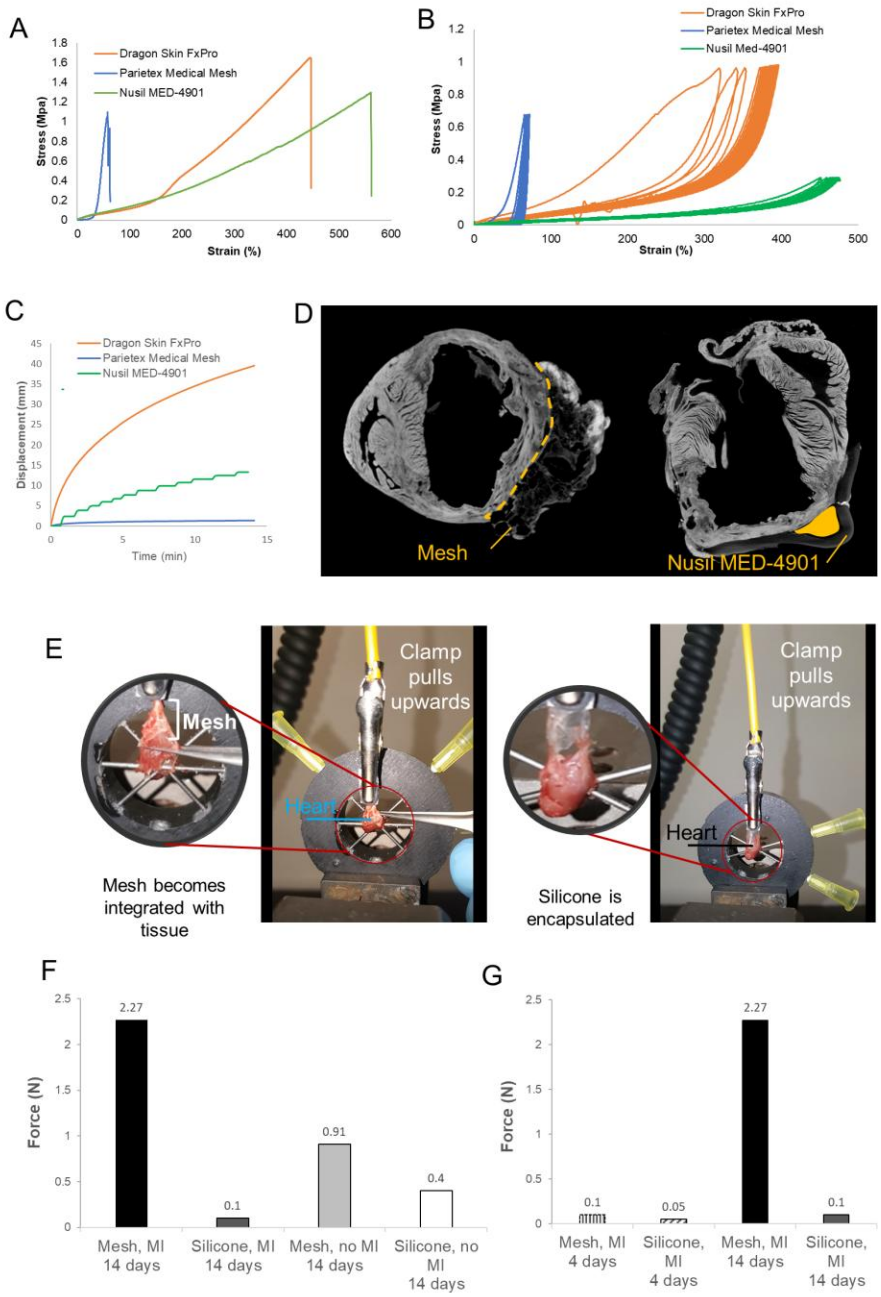

Figure 7: Material properties and adhesion strength characterization of potential interface materials. A) Representative stress/strain curves for Dragon Skin FX-Pro, medical mesh and MED-4901. B) Cyclical test results (20 cycles) for each material. C) Creep test (averaged for n=5) for each material. D) Representative image of μCT reconstruction of mesh and silicone, showing superior conformability of the mesh to the heart surface. Yellow dashed line shows device/tissue interface. Solid yellow shows separation area of the silicone from the heart. E) Pull-off failure mechanism. Mesh detaches in a stepwise fashion, and is more integrated to the tissue, while silicone is encapsulated, and slides off. F) Maximum pull-off forces for MI and healthy models at

day 14. G) Maximum pull-off force in the MI model for mesh and silicone at 4d and 14d time-points.

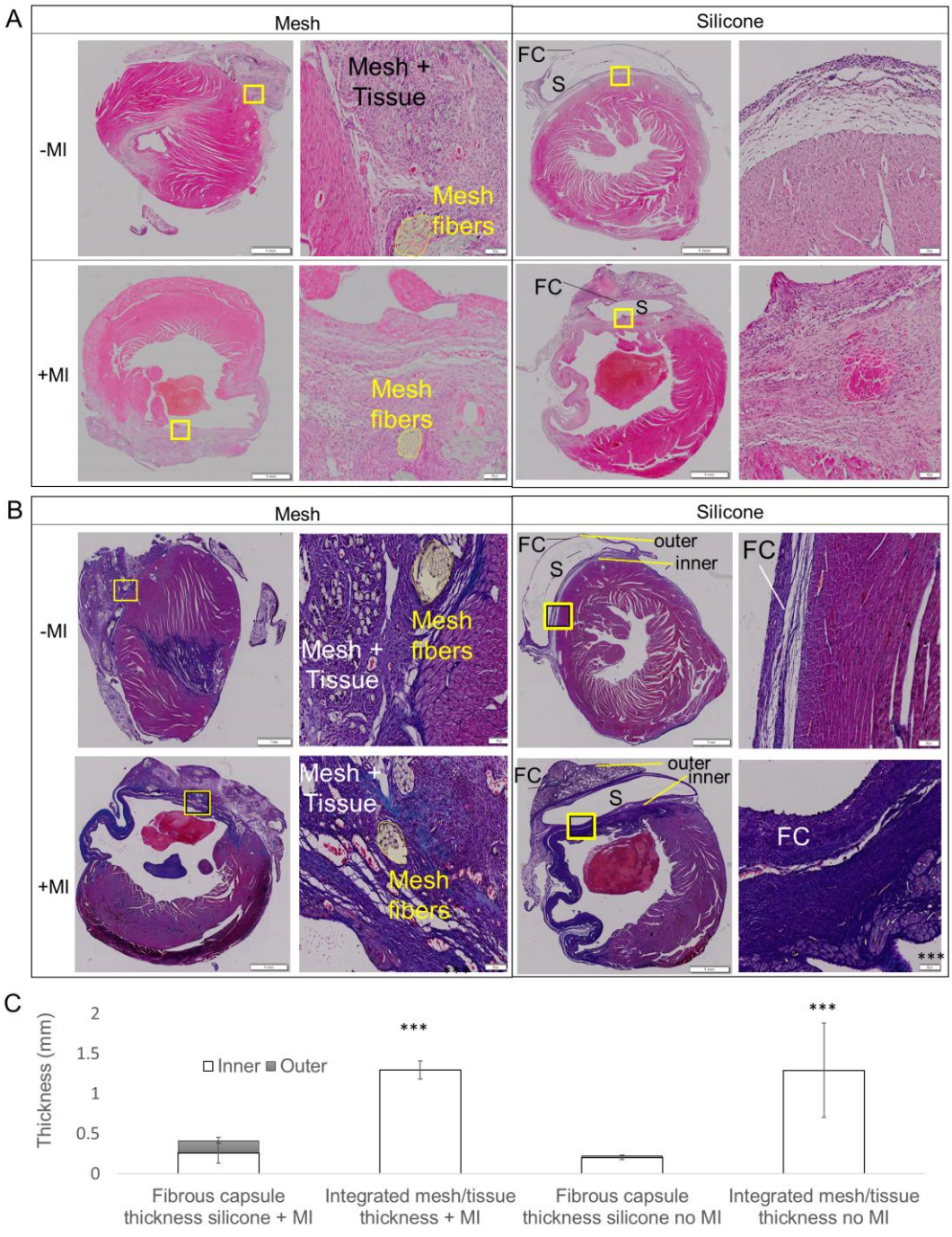

Figure 8: Histological analysis from *in vivo* murine study. A) H&E staining, B) Masson's Trichrome staining. FC=fibrous capsule, S=silicone, Inner = inner fibrous capsule, closest to epicardium, Outer=outer fibruous capsule, outside silicone implant. C) Quantification of tissue host response thickness – granulation tissue for the mesh and fibrous capsule for the silicone implant. (inner = in contact with epicardium, outer = not in contact with epicardium). Yellow square insets are magnified in right-hand panels. Data are mean ±

SD, ***p<0.0001, a one-way ANOVA with Sidak's multiple comparison post-hoc test was used. The integrated tissue/mesh thickness was compared to the total fibrous capsule thickness for the silicone groups with and without MI.